End-To-End Uncertainty Quantification with Analytical Derivatives for Design Under Uncertainty

Ben D. Phillips* and Joanna Schmidt[†] NASA Langley Research Center, Hampton, VA, 23666

Robert D. Falck [‡] and Eliot D. Aretskin-Hariton [§] *NASA Glenn Research Center, Cleveland, OH, 44135*

Uncertainty quantification (UQ) is a rapidly growing and evolving discipline, especially within the aerospace community. Performing analysis with UQ can provide decision makers with a wealth of information about a candidate design. However, the value of UO is fully realized when the information gained during UQ analysis is leveraged in a feedback loop of a design optimization process, often referred to as design under uncertainty. Although design under uncertainty can be a powerful risk mitigation technique, there are a number of roadblocks that prevent its implementation. Two primary factors are computational costs and added complexity of the analysis. High fidelity simulations having on the order of tens of uncertain variables quickly become computationally infeasible. Also, implementing UQ into an existing multidisciplinary design and optimization (MDO) process often requires extensive knowledge of the UQ methods and careful treatment of the problem formulation. The objective of this work is to address these two primary roadblocks and enable practitioners to efficiently perform design under uncertainty with limited knowledge of the UQ discipline. Methods outlined in this paper demonstrate MDO incorporating UQ into the design process, leveraging an analytical derivative tool chain through the entire optimization. The proposed approach leverages machine learning techniques to generate a differentiable confidence interval output from polynomial chaos models. This technique, coupled with the incorporation of analytical derivatives through the Polynomial Chaos Expansion (PCE) process, eliminates the need to estimate derivatives, which are usually obtained from finite difference, complex step, or similar methods. Developing a differentiable confidence interval allows mixed uncertainty problems (both epistemic and aleatory) to be modeled. Without such modeling, these problems cannot accurately predict objective functions containing statistical quantities such as mean and variance. The addition of analytical derivatives to a UQ method based on polynomial chaos can decrease the computational costs of performing design under uncertainty by orders of magnitude in comparison with methods such as complex step. The method and codes developed are modular in nature and are a drop-in solution for design under uncertainty within existing MDO problems. Low-fidelity analytical multidisciplinary optimizations under uncertainty for a wing design in OpenMDAO are detailed in this paper. These demonstration cases includes both objective functions and constraints which are influenced by uncertain parameters. Results show an 87.7% reduction in computational costs compared to current methods. Comparison of deterministic and uncertain designs shows significant improvement for the quantity of interest when the optimizer is given information about the uncertain space.

^{*}Aerospace Engineer, Aeronautics Systems Analysis Branch, Systems Analysis and Concepts Directorate.

[†]Aerospace Engineer, Aeronautics Systems Analysis Branch, Systems Analysis and Concepts Directorate.

[‡]Aerospace Engineer, Mission Architecture and Design Branch.

[§] Aerospace Engineer, Propulsion Systems Analysis Branch.

Nomenclature

AR	Wing Aspect Ratio	P_{minx}	Chord wise Location of Minimum Pressure
A_i	Undetermined PCE Coefficients	p	Order of PCE Model
a	Significance Level	\mathcal{R}_z	Residual of Implicit Output, z
b	Span	S_w	Wing Area
C	Camber	S_{csw}	Control Surface Area
$C_{l_{lpha}}$	Wing Section Lift Curve Slope	t/c	Wing Thickness-to-Chord Ratio
$C_{l_{lpha 0}}$	Wing Section C_l at $a = 0$	$ec{m{U}}$	Uncertainty Space
$C_{L_{lpha}}$	Wing Lift Curve Slope	V	Velocity
C_L	Wing Lift Coefficient	W_{dg}	Flight Design Gross Weight
C_{D_0}	Wing Zero Lift Drag Coefficient	W_{wing}	Wing Weight
C_{D_i}	Wing Induced Drag Coefficient	W_{total}	Total Vehicle Weight
C_{D_w}	Wing Wave Drag Coefficient	W_{fuel}	Fuel Weight
C_D	Wing Total Drag Coefficient	W_{base}	Base Vehicle Weight
c_r	Wing Root Chord	\vec{x}	Vector of Resampled PCE Values
d	PCE Deterministic Variables	ξ	PCE Random Variables
F	PCE Response	Z	PCE Confidence Interval Bound
$ar{f}$	Activation Function	$\%_L$	Percentage of Laminar Flow
g	Gravity Constant	α	Angle of Attack
$ec{m{j}}$	Design Variables	β	Mach Correction
\vec{K}	Constraint Functions	κ_{α}	Korn Factor
L	Lift	λ	Wing Taper Ratio
M	Mach Number	Λ	Wing Leading Edge Sweep Angle
N_t	Number of Terms Necessary for PCE Model	μ	Mean
N_z	Ultimate Load Factor	Ψ_i	PCE Basis Functions <i>i</i> th Mode
n	Number of Uncertain Parameters in PCE Model	σ	Standard Deviation
n_{an}	Function Calls for Analytical Derivatives	$\sigma_{C_{D_0}}$	Drag Multiplication Factor
n_{dv}	Function Optimization Design Variables	σ_{C_L}	Stall Loss of Lift Factor
n_{fd}	Function Calls for Finite Difference	ω	Activation Function Tuning Parameter
n_{pce}	Function Calls for PCE at Each Step		
\dot{P}	Number of Terms in PCE Model		

I. Introduction

MDO tools and methods have rapidly advanced the state-of-the-art over the last decade. Notably, the NASA-developed software, OpenMDAO [1], has provided the community an open-source, modular code built on a modern code architecture. A recently completed Technical Challenge (TC) in the Transformational Tools and Technologies (TTT) Project established gradient-based MDO that leverages analytical derivatives as a foundational approach throughout NASA's Aeronautics Research Mission Directorate (ARMD). The motivation of the research contained in this paper is to extend the gradient-based MDO with analytical derivatives to uncertainty quantification and design under uncertainty. This work will address the two primary roadblocks to uncertainty quantification adoption (computational cost and problem complexity) and enable practitioners to efficiently perform design under uncertainty with limited knowledge of uncertainty quantification (UQ). Integrating UQ into aircraft preliminary design is of particular interest to NASA. Assessing the impact of uncertainties early in the design process can help guide higher fidelity analysis and potentially prevent sub-optimal vehicle performance. The example cases laid out in this paper demonstrate the methodology on optimizations which tailor designs for optimal confidence-interval-based predicted performance estimates.

The rest of the paper is organized as follows: Section II covers the uncertainty modeling methodology using polynomial chaos and the assessment of analytical gradients through each step of the process. Section III applies the methodology to a wing optimization case study. The wing itself is composed of aerodynamics, weights, and range subsystems which are covered in Sections III.A, III.B, and III.C, respectively. The optimization problem formulation for the case study and the results are detailed in Sections III.E and III.F. Finally, conclusions are presented in Section IV.

II. Methodology

This section is divided into two subsections: the first section focuses on the underlying uncertainty modeling methodology, and the second section introduces the approach to obtain analytical derivatives for the confidence interval generated from a polynomial chaos model.

A. Uncertainty Quantification Methodology

Generally speaking, UQ encompasses the study of the impact of uncertainties in input parameters and modeling simplifications on the outputs or responses of a process or simulation. UQ can vary in scope by including only a single model or multiple models of varying fidelity levels as well as experimental data. The overarching objective of UQ is to create a more robust design or evaluation process by identifying sensitivities and mitigating the potential impact of uncertainties through informed, targeted resource investments. Two main types of uncertainty are present in most simulations: model input uncertainty and model form uncertainty. An important facet of UQ is the proper characterization and treatment of the simulation input uncertainties [2, 3].

1. Second-Order Probability

To propagate uncertainty through the model, the second-order probability approach outlined by Eldred and Swiler [4] for the treatment of mixed aleatory and epistemic uncertainties was employed. A flowchart of the method is shown in Fig. 1.

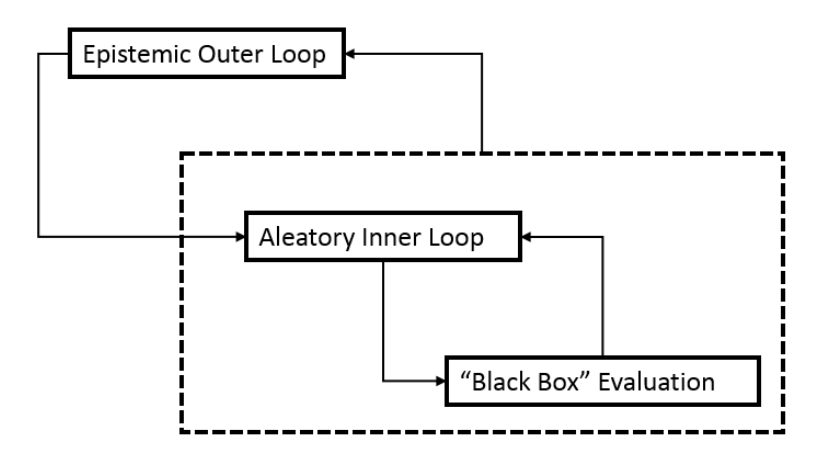


Fig. 1 Second-order probability architecture.

For each set of epistemic uncertainties, a cumulative distribution function (CDF) can be generated from the set of associated aleatory uncertainties as seen in Fig. 2. The probability box (P-Box) plot shows the family of CDFs generated from the second-order probability approach. To determine a 95% uncertainty interval on the response of interest, the lowest response value is extracted from a CDF at the 2.5% probability level and the highest response value is extracted from a CDF at the 97.5% probability level for a significance level of a=0.05. The use of the P-Box uncertainty approach is conservative, but it is statistically justifiable for the given inputs to the simulations. Note that the choice of significance level is somewhat subjective and can alter the findings.

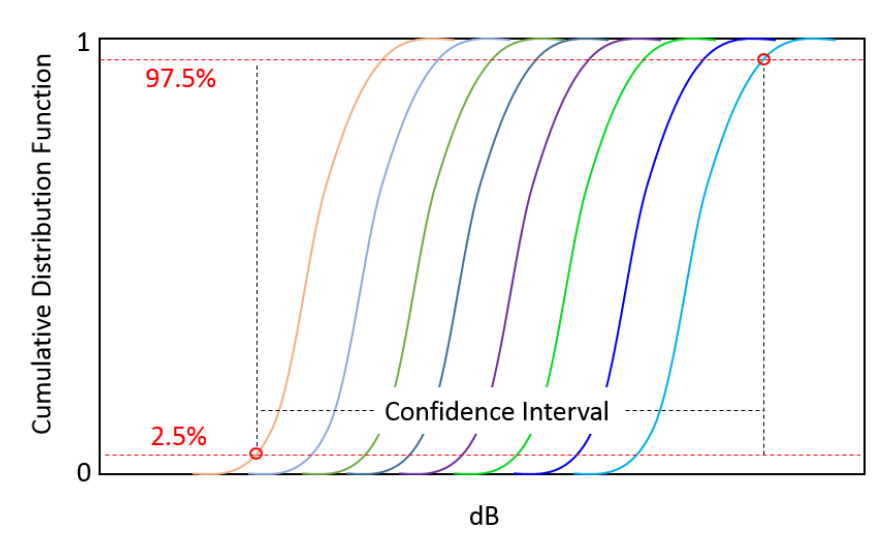


Fig. 2 Example P-Box.

2. Point-Collocation Non-intrusive Polynomial Chaos

A second method utilized in this research was non-intrusive polynomial chaos with point-collocation. Compared to traditional sampling methods such as Monte Carlo, the polynomial chaos method has been demonstrated as a viable and economical means of uncertainty quantification for CFD-based applications [5]. Polynomial chaos is a surrogate modeling technique based on a spectral representation of uncertainty. An important aspect of spectral representation of uncertainty is that a response value or random function, F, can be decomposed into separable deterministic and stochastic components, as shown in Eq. (1).

$$F(\boldsymbol{d},\boldsymbol{\xi}) \approx \sum_{i=0}^{P} A_i(\boldsymbol{d}) \Psi_i(\boldsymbol{\xi})$$
 (1)

Here, A_i is the deterministic component and Ψ_i is the random variable basis functions corresponding to the i^{th} mode. The basis functions, Ψ_i , of each random variable are determined using the Askey key [6] and are dependent on the distribution of each random variable. The response, F, is a function of independent, random variables, ξ , and deterministic variables, d. This series is in theory an infinite series but is truncated in practice. To form a complete basis or for a total order expansion, N_t terms are required, which can be computed from Eq. (2) for a polynomial chaos expansion (PCE) of order p and a number of random dimensions or variables, n.

$$N_t = P + 1 = \frac{(n+p)!}{n!p!} \tag{2}$$

Further details on polynomial chaos theory are given by Refs. [5, 7–9]. To compute the expansion coefficients, A_i , a point-collocation method is utilized [5]. The response, F, is sampled at locations throughout the random variable space, and the expansion coefficients are computed with an over-determined, least squares approach. At least N_t samples are needed for this procedure; Hosder et al. recommend an oversampling ratio of two (i.e., $2 \cdot N_t$ samples). In some models where not all terms are significant, it is possible to build the PCE model with fewer than N_t samples. A process such as backward elimination [10] could be utilized to build such a model.

3. Uncertainty Quantification with Polynomial Chaos Expansion (UQPCE)

All of the uncertainty modeling and analysis contained in this research was performed with one of NASA's in-house uncertainty codes, Uncertainty Quantification with Polynomial Chaos Expansion, UQPCE [11]. UQPCE is an open source, Python-based research code for use in parametric, non-deterministic computational analysis and design. UQPCE utilizes a non-intrusive polynomial chaos expansion surrogate modeling technique, as outlined above in Section II.A.2, to efficiently estimate uncertainties for computational analyses. The software enables the user to perform an automated uncertainty analysis for any given computational code without requiring modification to the source. UQPCE estimates

sensitivities, confidence intervals, and other model statistics which can be useful in the conceptual design and analysis of flight vehicles. This software was originally developed with funding from the Commercial Supersonic Technology (CST) Project to study the potential impacts of uncertainties on the prediction of ground noise generated from commercial supersonic aircraft concepts [12–15]. The code development is currently supported by the TTT project and has been leveraged in uncertainty analysis for electrified aircraft propulsion studies [16].

B. Analytical Derivatives for PCE-Generated Confidence Intervals

To employ a PCE approach in a gradient-based design under uncertainty MDO problem, a PCE model must be assembled at each point within the design space (i.e., each step the optimizer takes). However, each PCE model only gives estimates for statistical parameters (e.g., mean, variance, confidence intervals, sensitivities, etc.) at that step. As noted in Ref. [8], the PCE models at each step are only valid for those particular values of design variables and must be recalculated when the design variables are changed. To estimate derivatives at each step with a method such as finite difference, multiple PCE models are necessary. The computational cost of these models scales with the order of the PCE expansion, number of uncertain parameters, and the number of design variables. For any moderately expensive underlying analysis, this process quickly becomes computationally intractable for cases with more than tens of design or uncertain parameters. Furthermore, when mixed uncertainty problems are being considered, a confidence-interval-informed objective function is required, which also adds non-negligible computational costs. Finite difference or complex step approximations of derivatives are often not computationally efficient options for incorporating uncertainty as constraints or objectives in an optimization. For these reasons, the authors propose an approach to generate analytical derivatives from PCE models. When paired with an MDO problem that has an entire analytical derivative tool chain, this approach can decrease computational costs by orders of magnitude.

Obtaining analytical derivatives of points on a confidence interval through a traditional process would involve differentiation through a binning procedure. In this work, instead of attempting to model the binning, an implicit function theorem and a smooth counting function are applied to generate an approximation that is sufficiently accurate when the number of data points involved is sufficiently large. First, some guess, z_{guess} , is assumed for the value of the upper bound of the confidence interval, z. In this paper, an activation function based on the hyperbolic tangent is used.

$$\bar{f}(\vec{x}, z, \omega) = 1 - \frac{\left(1 + \tanh(\frac{\vec{x} - z}{\omega})\right)}{2} \tag{3}$$

Equation (3) is effectively a continuous counting function that provides an approximate count of the number of elements in \vec{x} that are less than or equal to z. The parameter ω determines how abrupt the transition from 0 to 1 is in the vicinity near z. As ω approaches zero, the response more accurately models a step function, whereas larger values provide a smoother derivative. Figure 3 shows the PDF, CDF and associated activation function for a normal distribution. The vertical dashed lines in the figure represent the chosen significance level for the confidence interval and the corresponding location on the PDF, CDF, and activation function.

For a selected significance level a equal to 0.05, 95% of the data fall within the confidence interval, with 2.5% falling above the upper end of the interval. The residual equation that governs the value of the 95% confidence interval, z, is thus:

$$\mathcal{R}_z(\vec{x}, z, \omega) = \sum_{i=1}^n \bar{f}_i(\vec{x}, z, \omega) - 0.975n$$
 (4)

The partial derivatives for the residual with respect to both \vec{x} and z are needed. Although these derivatives can be approximated using finite difference or complex step, it is not uncommon for \vec{x} to have a length on the order of millions; approximating the derivatives quickly becomes expensive. The analytical derivatives below are provided to OpenMDAO to avoid unnecessary computational expense.

$$\frac{\partial \mathcal{R}_z(\vec{x}, z, \omega)}{\partial x} = \frac{-1}{2\omega \cosh^2(\frac{\vec{x} - z}{\omega})}$$
 (5)

Normal Distribution

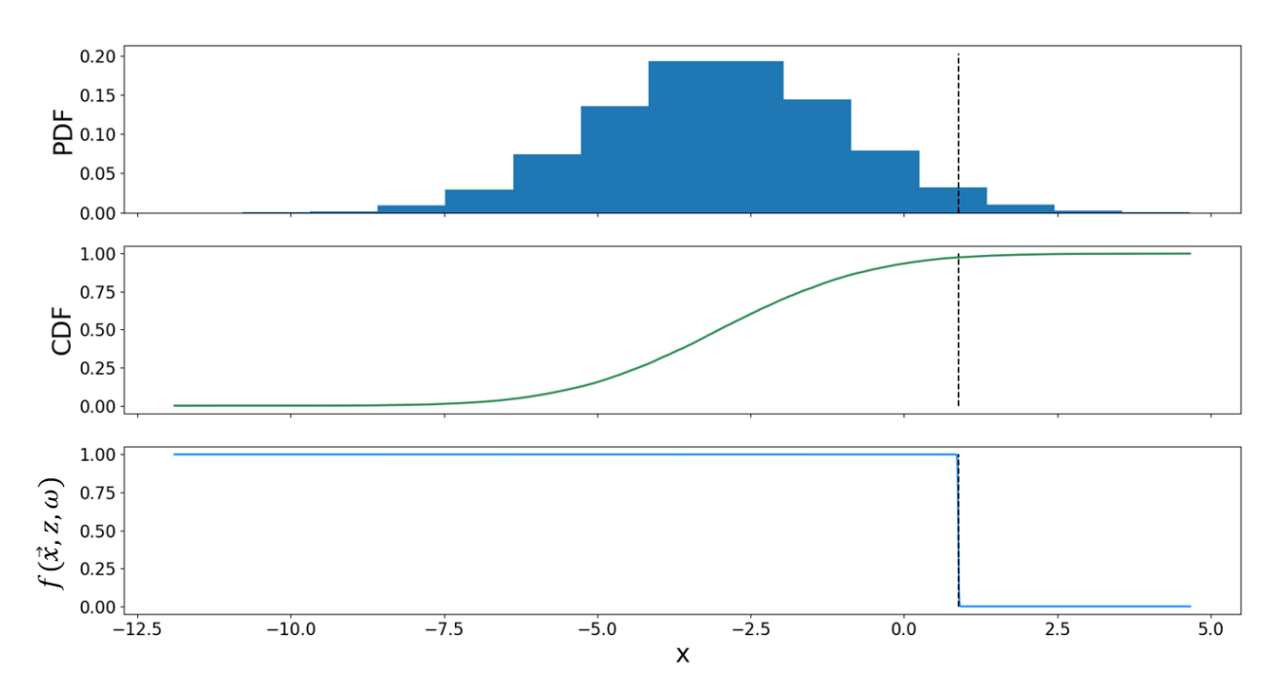


Fig. 3 Example PDF, CDF, and activation function of a normal distribution.

$$\frac{\partial \mathcal{R}_z(\vec{x}, z, \omega)}{\partial z} = \sum_{i=1}^m \frac{1}{2\omega \cosh^2(\frac{\vec{x} - z}{\omega})}$$
 (6)

Note that although the above implementation of analytical derivatives was used for the analysis in this case study, OpenMDAO now has the activation function implemented natively using the software package JAX[17] to calculate the derivatives. Equation 4 is differentiable with respect to z and can be efficiently solved using a Newton solver. To utilize z as an objective or constraint in gradient-based optimization, its total derivative with respect to the data \vec{x} needs to be computed. The software package OpenMDAO [1] is used to eliminate the residual using a Newton solver and then efficiently compute derivatives of z with respect to the data \vec{x} by applying the implicit function theorem to Eq. (4). Since R_z is a scalar value, this derivative can be evaluated with a single linear solve in reverse mode as opposed to n linear solves in forward mode. The hyperbolic tangent activation function can be susceptible to issues due to vanishing gradients when elements of \vec{x} are far from z, but the authors' experience using the mean and variance estimation output from the PCE model to inform the value of z_{guess} has lessened this concern. It is possible that more a priori information about the uncertainty space may be required if the location of the 95% confidence interval is significantly far away from the variance-informed value of z_{guess} shown in Eq. (7).

$$z_{guess} = \mu + 2\sigma \tag{7}$$

When epistemic uncertainties are present in a system, the bound on uncertainty is determined by finding the confidence interval from the outer lower and upper curves as shown in Fig. 2. Two steps are followed to find this bound on uncertainty while preserving the analytical derivatives throughout the calculation. First, the confidence interval of each individual curve is calculated following the above hyperbolic tangent method; this preserves the differentiability of the solved confidence interval values for all curves. Second, the minimum or maximum of these individual confidence intervals is calculated using OpenMDAO's implementation of the Kreisselmeier-Steinhauser (KS) function. This results in a differentiable bound on the uncertainty for a system that includes both aleatory and epistemic uncertainties. This technique coupled with the incorporation of analytical derivatives through an MDO process eliminates the need to

estimate derivatives, which are usually derived from finite difference, complex step, or similar methods. Developing a differentiable confidence interval allows mixed uncertainty problems to be modeled where previous methods were unable to represent objective functions containing statistical quantities such as mean and variance.

The cost per iteration of running a gradient-based optimization incorporating uncertainty with PCE and finite difference to estimate gradients, n_{fd} , is given by Eq. (8).

$$n_{fd} = n_{pce}(n_{dv} + 1) \tag{8}$$

where n_{pce} is the number of terms necessary to build the PCE model and n_{dv} is the number of design variables in the optimization (note that n_{pce} is equivalent to N_t in Eq. (2), and in practice, $2N_t$ or $2n_{pce}$ are generally used.) Conversely, the cost per iteration of running a gradient-based optimization incorporating uncertainty with PCE and analytical gradients to obtain gradients, n_{an} , is given by Eq. (9).

$$n_{an} = n_{pce} (9)$$

From Eqs. (8) and (9), the cost savings of design under uncertainty for gradient-based optimization leveraging analytical gradients through PCE scales with the product of the number of terms necessary to build the PCE model and the number of design variables, $n_{pce}n_{dv}$. The addition of analytical derivatives to a polynomial-chaos-based UQ method can decrease the computational costs of performing design under uncertainty by orders of magnitude in comparison with methods such as finite difference or complex step.

III. Case Study

This case study is an academic exercise of the methodology on a multidisciplinary optimization under uncertainty. A wing design case was chosen as a relevant application for aerospace multidisciplinary design. This case study is not an attempt to capture all relevant physics and design considerations for an aircraft wing. Rather, this work will demonstrate the tools and methods developed on a problem of interest for conceptual design, leveraging "textbook methods" for minimal computational costs and ease of visualization of the design space. Two separate optimizations are detailed in this paper, one for maximum lift-to-drag ratio (L/D), and a second for maximum range. The design parameters and uncertain parameters differ for each. All design parameters and uncertain parameters are listed in this Section (refer to Section III.E for details). The design variables for the optimizations are given in Table 1, and the uncertain parameters are given in Tables 2 and 3. The following sections will discuss the various disciplines and analysis incorporated in this case study.

Table 1 Design variables

Input	Range	Optimization
t/c	[0.1, 0.15]	Both
P_{minx}	[0.3, 0.5]	Both
C	[0.01, 0.043]	Both
α	[-8, 14](deg)	L/D Only
λ	[0.1, 1]	Both
Λ	[0, 40] (deg)	Both
b	[20, 50] (m)	Both
c_r	[5, 7](m)	Both

Table 2 Uncertain parameters (epistemic)

Input	Interval	Optimization
$\%_L$	[0, 25%]	Both
$\sigma_{C_{D_0}}$	[4, 6]	Both
κ_{α}	[0.85, 0.95]	Both
S_{csw}	[0.05, 0.2]	Range Only

Table 3 Uncertain parameters (aleatory)

Input	Distribution	Mean	Std. Dev.	
σ_{C_L}	Gaussian	$2x10^{-5}$	$3x10^{-6}$	Both
M	Gaussian	0.72	0.02	Both
c_t	Gaussian	0.45	0.045 (1/hr)	Range Only

A. Aerodynamics

Aerodynamic calculations for lift and drag are implemented from analytic, low fidelity methods. Only lift and drag are considered in this case study. First, 72 NACA 6-series airfoils of varying thickness and camber were run through a 2-D panel code[18] to estimate their sectional lift curve slope and lift at $\alpha=0$ values. Then, a regression model was assembled from the data to fit characteristics from the NACA 6-series (location of minimum pressure, P_{minx} , thickness-to-chord ratio, t/c, and camber, C) to the sectional lift values. This process allowed the optimizer to have continuous design variables that influenced the sectional lift properties.

$$C_{lo} = f(P_{minx}, t/c, C) \tag{10}$$

$$C_{l_{\alpha_0}} = f(P_{minx}, t/c, C) \tag{11}$$

A knockdown factor of 0.5 was applied to $C_{l_{\alpha_0}}$ to take into account 3-D wing effects. The factor of 0.5 was chosen to match aerodynamic performance data for 737 class vehicles.

$$C_{L_{\alpha_0}} = 0.5C_{l_{\alpha_0}} \tag{12}$$

The wing lift curve slope, $C_{L_{\alpha}}$, from Ref. [19] is given in Eq. (13) below. This formula takes into account compressibility, sweep, and finite span effects.

$$C_{L_{\alpha}} = \frac{2\pi AR}{2 + \sqrt{4 + \frac{AR^2\beta^2}{n^2} (1 + \tan^2(\Lambda)/\beta^2)}}$$
(13)

where β and η are given by:

$$\beta = \sqrt{1 - M^2} \tag{14}$$

$$\eta = \frac{C_{l\,\alpha}}{2\pi/\beta} \tag{15}$$

The lift coefficient then becomes:

$$C_L = C_{L_{\alpha_0}} + C_{L_{\alpha}}\alpha - \sigma_{C_L}\alpha^4 \tag{16}$$

The last term of Eq. (16) contains an uncertain parameter, σ_{C_L} , that models the stall loss of lift at higher angles of attack. To calculate the skin friction drag or zero lift drag, flat plate equations [20] were utilized:

$$C_{fL} = \frac{1.328}{\sqrt{Re_L}} \tag{17}$$

$$C_{f_T} = \frac{0.455}{\log(Re_L)^{2.58}(1 + 0.144M^2)^{0.65}}$$
 (18)

The zero lift drag coefficient is then estimated by:

$$C_{D_0} = 2(C_{f_L}\%_L + (1 - \%_L)C_{f_T})\sigma_{C_{D_0}}$$
(19)

where the uncertain parameter, $\%_L$, denotes the percentage of expected laminar flow over the wing. The factor of two represents drag on both "sides" of the flat plate (upper and lower wing surface). $\sigma_{C_{D_0}}$ is an uncertain parameter that multiplies the zero lift drag of the wing to estimate a value for the theoretical full vehicle. The range of $\sigma_{C_{D_0}}$, [4, 6], translates to the wing accounting for roughly 17% to 25% of the overall theoretical full vehicle zero lift drag. Equations to determine the wing efficiency, which is an input into the induced drag calculation, are based on historical data, and regression models are given by Pamadi [21] in Eqs. (20), (21), and (22). These equations take into account wing aspect ratio, leading edge sweep, taper ratio, and section lift coefficient.

$$\kappa = \frac{AR\lambda}{\cos\Lambda} \tag{20}$$

$$r = 0.0004\kappa^3 - 0.008\kappa^2 + 0.05\kappa + 0.86$$
(21)

$$e = \frac{1.1C_{L_{\alpha}}}{rC_{L_{\alpha}} + (1 - r)\pi AR} \tag{22}$$

The induced drag, C_{D_i} , is then calculated by:

$$C_{D_i} = \frac{C_L^2}{\pi \varrho A R} \tag{23}$$

The wave drag, C_{D_w} , is given by:

$$C_{D_{vv}} = 20(M - M_{cr})^4 \tag{24}$$

where the critical Mach number, M_{cr} , is:

$$M_{cr} = M_{DD} - \frac{0.1^{1/3}}{80} \tag{25}$$

and the drag divergence Mach number, M_{DD} , is given by:

$$M_{DD} = \frac{\kappa_{\alpha}}{\cos \Lambda - \frac{t/c}{\cos \Lambda^2} - \frac{C_L}{10\cos \Lambda^3}}$$
 (26)

The Korn factor, κ_{α} , [22] was included as an uncertain parameter (see Table 3). The total drag is given by the summation of the zero lift drag, induced drag, and wave drag.

$$C_D = C_{D_0} + C_{D_i} + C_{D_w} (27)$$

B. Weights

Wing weight formulations were used in the optimization both as a constraint and as part of an objective function in two separate optimizations. An empirical method based on historical data and regression estimations given by Raymer [19] (imperial units) was employed. This equation takes into account all the wing planform characteristics and estimates an empty wing mass based on historical data.

$$W_{wing} = 0.0051(W_{dg}N_z)^{0.557}S_w^{0.649}AR^{0.5}t/c^{-0.4}(1+\lambda)^{0.1}\cos(\Lambda)^{-1}S_{csw}^{0.1}g$$
(28)

A control surface area, S_{csw} , of 10% was estimated for L/D optimization (see Section III.E) and treated as an uncertain parameter for the range optimization. The weight for the remaining vehicle, W_{base} , (empty operating weight plus passengers and cargo minus fuel and wing weight) was set as a constant of 63,000 kg. This value was chosen to align the data in the demonstration case to roughly to a 737-8 class vehicle.

$$W_{total} = W_{wing} + W_{fuel} + W_{base} (29)$$

C. Range

Vehicle range was only calculated in the optimization problem maximizing range. The Breguet range equation [23] for a cruise climb was implemented.

$$R = \frac{V}{c_t} \frac{L}{D} \ln \frac{W_0}{W_1} \tag{30}$$

Thrust specific fuel consumption (TSFC), c_t , was treated as an uncertain parameter (see Table 3). A fuel mass of 17,500 kg $(W_0 - W_1)$ was set as a constant and the start of cruise altitude was set at 35,000 ft.

D. Iterative Force Balance

During the range optimization process, each iteration produces a wing design with a corresponding weight. In the demonstration optimizing range, angle of attack is not a design variable, but a solver variable (see III.E for more details). To get an accurate prediction of range, the vehicle must be trimmed so that L=W. The example problem utilizes a Newton solver coupled with an OpenMDAO balance component to solve for the α value that produces the necessary lift to balance weight. The solved α values are then passed along to the drag calculation and propagated through the rest of the problem.

E. Optimization Problem Formulations

To demonstrate the design under uncertainty methodology, two optimizations were performed. An example extended Design Structure Matrix (XDSM) of an optimization incorporating the calculations in the above sections is shown in Fig. 5 below. In this work, we adopt the convention of the † superscript for input or outputs containing uncertain parameters and the purple color for blocks where uncertainty analysis is performed. Subscripts $_{CI}$ indicate a confidence interval value estimated from a UQPCE analysis.

1. Simplified Optimization Problem: L/D

The first optimization problem focused on maximizing L/D, utilizing only aerodynamics and weights subsystems (Sections III.A and III.B). In this optimization, the lower 95% confidence interval for the L/D is maximized subject to a maximum wing weight constraint. The arbitrary wing weight constraint was enforced to prevent the wing from sizing unrealistically heavy. This simple example enables comparisons back to a deterministic optimization for the same response. For the deterministic optimizations, the uncertain parameters were fixed at their mean in the case of aleatory uncertainties or central value in the case of epistemic uncertainties. Note that the uncertain parameters c_t and S_{csw} in Tables 2 and 3 were not included in this simplified case. The formulation of this optimization problem is given by:

Maximize L/D

Subject to Weight Constraint: $W_{wing} < 6000 kg$

An XDSM of this simplified optimization is given in Fig. 4.

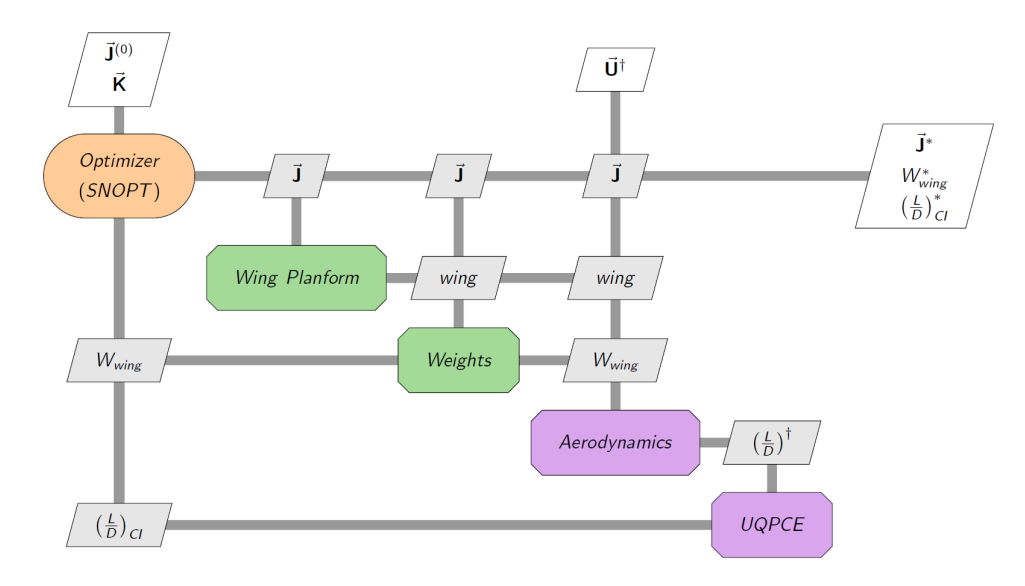


Fig. 4 XDSM of simplified optimization.

2. Extended Optimization Problem: Range

The second optimization incorporated all the disciplines and targeted maximizing the lower 95% confidence interval of range. A constraint was imposed on minimum lift generation during cruise to ensure sufficient lift generation to balance weight. This constraint was imposed to ensure solver convergence outlined in Section III.D. The formulation of this optimization problem is given by:

Maximize Range

Subject to Lift Constraint : $L_{max} > W_{total}$

For each optimization, the user provides design variables, ranges, and initial guesses, (\vec{J}^*) , and constraints, (\vec{K}) . Then the initial wing planform is calculated. Next, the optimizer feeds the wing planform into the weights analysis block which produces a weight estimate that is returned to the optimizer. Then, the wing design is passed to the aerodynamics analysis along with the uncertainty space. The first, simplified example case returns the L/D parameter to the optimizer and iterates until convergence. The second, expanded example case contains a UQPCE block which wraps a Newton solver and the aerodynamics block in a subproblem where α is iterated to balance L and W_{total} . Note that the output from the subproblem is a vector of lift values, which in turn produces a vector of solved α values. The minimum lift constraint value, L_{max} , is also calculated in the aerodynamics block and passed back to the optimizer. The solved α vector is used to calculate drag, which along with lift, is passed to the range calculation block. PCE models are assembled from the UQPCE block from the vectors of lift and drag. Similar to the aerodynamics block, another UQPCE block wraps the range calculation in a subproblem and produces a vector of range values which are used to generate the PCE model for the range response. Finally, the lower 95% confidence interval for range is fed back to the optimizer as the objective function. The optimizer iterates on the design variables until convergence is achieved. For this formulation of the problem, it is not explicitly necessary to solve for α in this manner. However, the forward propagation of uncertainty becomes easier to model with this approach.

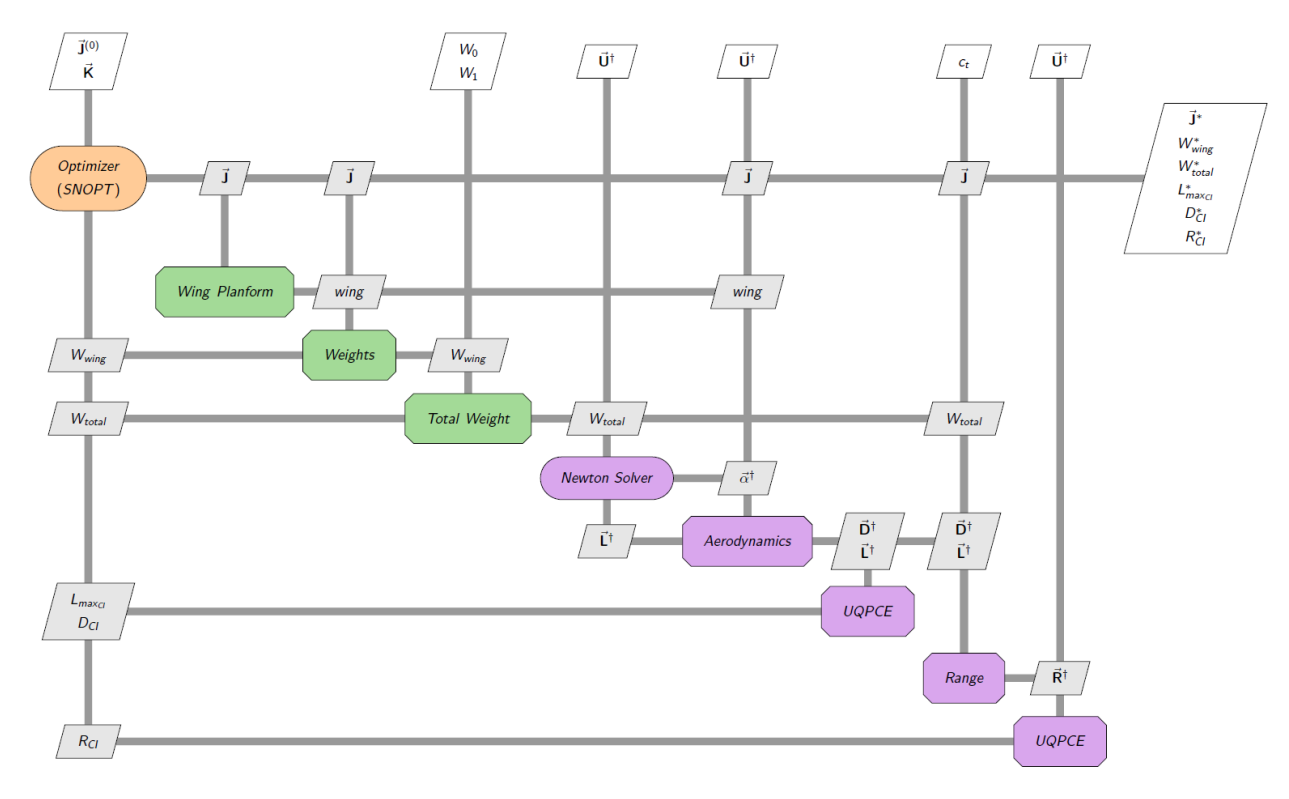


Fig. 5 XDSM of full optimization.

F. Results

This section details the results from both optimizations in this case study. The simplified example optimizing L/D will be discussed first. Then the second, more complex example, which focused on optimizing range, will be detailed.

1. Simplified Optimization Problem: L/D

The simplified example was chosen as a demonstration case for easy comparison between a deterministic optimization and an optimization under uncertainty. The resultant design variable outputs for these optimizations are given in Table 4. Note that the constraint of maximum wing weight was active for both the deterministic and uncertain cases. This is expected as the optimizer would prefer to drive the wing larger (bigger span) to reduce induced drag thereby increasing L/D.

Table 4 Comparison of design variable output from uncertain and deterministic optimizations

Variable	L/D_{CI} (Uncertain)	L/D (Deterministic)
t/c	0.1	0.115
P_{minx}	0.317	0.3
C	0.043	0.043
α	3.888 (deg)	3.349 (deg)
λ	0.238	0.223
Λ	37.15 (deg)	26.86 (deg)
c_r	5 (m)	5 (m)
b	30.33 (m)	34.84 (m)

A visual comparison of the optimal wing designs is shown in Fig. 6. The most visible difference is the sweep angle between the two wings. The uncertain optimization (red) added more sweep to counter the impact of increased wave drag at the higher end of the Mach number uncertain range (see Eq. (24) through Eq. (26). To balance the increased weight from a higher leading edge sweep angle (see Eq. (28)), the span was decreased.

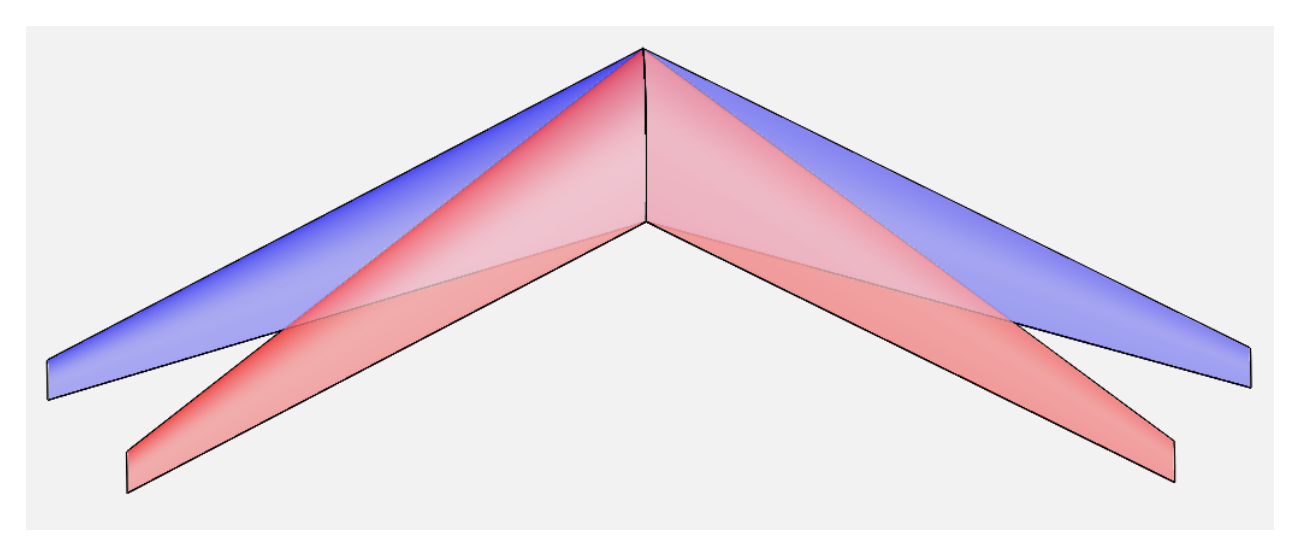


Fig. 6 Comparison of optimal planform designs (deterministic in blue, uncertain in red).

The confidence intervals and mean values from the resultant optimizations are given in Table 5.

Table 5 Comparison of results from uncertain and deterministic optimizations.

Variable	L/D_{CI} (Uncertain)	L/D (Deterministic)
Mean	15.73	18.073
Confidence Interval	[12.71, 18.74]	[8.031, 21.03]

The optimal design for the deterministic case produces a higher mean (or central value due to the presence of epistemic uncertainty) L/D value than the uncertain case, 18.07 versus 15.73. However, at the optimal point for the deterministic solution, the lower confidence interval for L/D is significantly lower than the corresponding value on the uncertain graph, 8.031 versus 12.71. Interpreting these results, the uncertain optimization has taken into account the uncertainty within the design space and tailored the wing planform design to mitigate against the probability of an extremely low L/D response. In this case, if this wing were designed without considering uncertainty, there would be a probability of encountering significantly lower L/D values, even though the mean value outperforms that of the uncertain design. This demonstrates a common outcome when performing design under uncertainty - trading a less desirable mean value of the quantity of interest for more desirable "worst-case" value of the quantity of interest.

2. Extended Optimization Problem: Range

The resultant design variable outputs for deterministic and uncertain optimizations are given in Table 6. Note that the constraint of minimum lift was not active for either the deterministic or uncertain cases. Table 6 indicates the major difference between the two designs is the leading edge sweep angle. Similar to the first, simplified case, the uncertain design resulted in a wing with more sweep. Note that the wing weight is a fallout calculation from the planform and is non-deterministic for the uncertain case given the uncertain parameters in the analysis (See Tables 2 and 3).

Although this demonstration case is not a direct comparison between uncertain and deterministic optimization due to the abstraction of the uncertainty space, a small benefit was realized. The uncertain optimization was able to produce roughly a 10.2% increase in the lower confidence interval estimate for range while producing a marginally smaller predicted mean value (1.2%). As shown in Table 6 the uncertain optimization produced a wing with a significantly

Table 6 Design and output parameters from optimization with uncertainty

Variable	range _{CI} Uncertain	range (Deterministic)
t/c	0.1	0.118
P_{minx}	0.312	0.3
C	0.043	0.043
λ	0.196	0.185
Λ	30.59 (deg)	24.32 (deg)
c_r	5 (m)	5 (m)
b	45.62 (m)	46.00 (m)
W_{weight}	9291.4 (mean, kg)	8338.0(kg)

Table 7 Comparison of results from uncertain and deterministic optimizations

Variable	range _{CI} (Uncertain)	range (Deterministic)
Mean	3679.6 (nmi)	3723.1 (nmi)
Confidence Interval	[2581.2, 5414.1] (nmi)	[2342.4, 5653.9] (nmi)

larger mass, 9291.4 kg vs 8338 kg. The optimizer chose to trade wing weight for better aerodynamic performance to increase the lower confidence interval for range.

Referring back to the Eqs. (8) and (9) in Section II, the cost savings to run this case can be estimated. This particular case required 53 iterations to converge, resulting in a theoretical total function call for finite-difference-based optimization of 30,952. With analytical derivatives for the same problem, the function call count becomes 3,816, a potential reduction of 87.7%.

IV. Conclusion

A framework for performing design under uncertainty leveraging polynomial chaos methods has been integrated into OpenMDAO. A demonstration case was presented showcasing the methodology. The developed code is extensible to any MDO analysis that can be formulated into an OpenMDAO-based analysis or design. Analytical gradients through polynomial chaos models enable orders of magnitude computational savings over finite difference or complex step in gradient-based optimization for design under uncertainty. The cost of optimization incorporating uncertainty has been decoupled from the number of design parameters in the problem. Constraints and objective functions can be formulated as either deterministic, uncertain, or combinations of both. The underlying polynomial chaos surrogate model is exposed to the user to enable an objective function of any statistical quantity desired. Future work will be focused on open source release of the code developed for this research, extensions of multifidelity analysis, demonstration cases with higher fidelity physics tools, and integration with the model-based systems analysis and engineering architectures.

V. Acknowledgements

The authors would like to thank Dr. Nicholas Borer and Dr. Nat Blaesser for their support in formulating the demonstration problem, as well as Mr. Brandon Litherland for his assistance generating airfoil models and graphics for this paper. This research was made possible by support from the Transformational Tools and Technologies Project (TTT) within the Transformative Aeronautics Concepts Program (TACP). Previous support for UQPCE development was funded by the Commercial Supersonic Technology Project (CST).

References

- [1] Gray, J. S., Hwang, J. T., Martins, J. R. R. A., Moore, K. T., and Naylor, B. A., "OpenMDAO: An open-source framework for multidisciplinary design, analysis, and optimization," *Structural and Multidisciplinary Optimization*, Vol. 59, No. 4, 2019, pp. 1075–1104. https://doi.org/10.1007/s00158-019-02211-z.
- [2] Walker, E. L., Hemsch, M. J., and West IV, T. K., "Integrated Uncertainty Quantification for Risk and Resource Management: Building Confidence in Design (Invited)," *53rd AIAA Aerospace Science Meeting*, AIAA 2015-0501, Kissimmee, Florida, 2015. https://doi.org/10.2514/6.2015-0501.
- [3] Oberkampf, W. L., and Roy, C. J., Verification and Validation in Scientific Computing, Cambridge University Press, New York, NY, 2010.
- [4] Eldred, M., and Swiler, L., "Efficient Algorithms for Mixed Aleatory-Epistemic Uncertainty Quantification with Application to Radiation-Hardened Electronics; Part I: Algorithms and Benchmark Results," Tech. Rep. SAND2009-5805, Sandia National Laboratories, September 2009.
- [5] Hosder, S., Walters, R. W., and Balch, M., "Point-Collocation Nonintrusive Polynomial Chaos Method for Stochastic Computational Fluid Dynamics," *AIAA Journal*, Vol. 48, No. 12, 2010, pp. 2721–2730. https://doi.org/10.2514/1.39389.
- [6] Xiu, D., and Karniadakis, G. E., "The Wiener-Askey Polynomial Chaos for Stochastic Differential Equations," SIAM Journal on Scientific Computing, Vol. 24, No. 2, 2002, pp. 619–644. https://doi.org/10.1137/S1064827501387826.
- [7] Ghanem, R. G., and Spanos, P. D., Stochastic Finite Elements: A Spectral Approach, Springer-Verlag, New York, NY, 1991.
- [8] Eldred, M. S., "Recent Advances in Non-Intrusive Polynomial Chaos and Stochastic Collocation Methods for Uncertainty Analysis and Design," 50th AIAA/ASME/ASCE/AHS/ASC Structures, Structural Dynamics, and Materials Conference, AIAA Paper 2009-2274, 2009. https://doi.org/10.2514/6.2009-2274.
- [9] Sudret, B., "Global Sensitivity Analysis Using Polynomial Chaos Expansion," *Reliability Engineering and System Safety*, Vol. 93, No. 7, 2008, pp. 964–979. https://doi.org/10.1016/j.ress.2007.04.002.
- [10] Montgomery, D. C., Design and Analysis of Experiments, 8th ed., Wiley, Hoboken, NJ, 2012.
- [11] Phillips, B. D., and Schmidt, J. N., "UQPCE v0.3.0," https://github.com/nasa/UQPCE, 2023.
- [12] Phillips, B. D., and West IV, T. K., "Trim Flight Conditions for a Low-Boom Aircraft Under Uncertainty," *Journal of Aircraft*, Vol. 56, No. 1, 2019, pp. 53–67. https://doi.org/10.2514/1.C034932.
- [13] Phillips, B. D., Heath, C., and Schmidt, J. N., "System-Level Impact of Propulsive Uncertainties for Low-Boom Aircraft Concepts," AIAA AVIATION 2020 Forum, AIAA 2020-2730, Virtual Event, 2020. https://doi.org/10.2514/6.2020-2730.
- [14] Endo, M., and Phillips, B. D., "Uncertainty Quantification of CFD Model Assumptions Against Sonic Boom Noise Prediction of a Commercial Supersonic Transport," *AIAA SCITECH 2022 Forum*, AIAA 2022-0401, San Diego, California, 2022. https://doi.org/10.2514/6.2022-0401.
- [15] Phillips, B. D., and West IV, T. K., "Aeroelastic Uncertainty Quantification of a Low-Boom Aircraft Configuration," 2018 AIAA Aerospace Sciences Meeting, AIAA 2018-0333, Kissimmee, Florida, 2018. https://doi.org/10.2514/6.2018-0333.
- [16] Kirk, J., Frederick, Z. J., Guynn, M. D., Blaesser, N. J., Phillips, B. D., Fisher, K., Schneider, S. J., and Frederic, P., "Continued Exploration of the Electrified Aircraft Propulsion Design Space," AIAA SCITECH 2023 Forum, AIAA 2023-1354, 2023. https://doi.org/10.2514/6.2023-1354.
- [17] Bradbury, J., Frostig, R., Hawkins, P., Johnson, M. J., Leary, C., Maclaurin, D., Necula, G., Paszke, A., VanderPlas, J., Wanderman-Milne, S., and Zhan, Q., "JAX: composable transformations of Python+NumPy programs,", ???? URL http://github.com/google/jax.
- [18] Drela, M., "XFOIL: An Analysis and Design System for Low Reynolds Number Airfoils," *Low Reynolds Number Aerodynamics*, Springer Berlin Heidelberg, 1989.
- [19] Raymer, D. P., *Aircraft Design: A Conceptual Approach*, 3rd ed., American Institute of Aeronautics and Astronautics, Inc, Reston, VA, 1999.
- [20] Bertin, J. J., and Cummings, R. M., *Aerodynamics for Engineers*, 5th ed., American Institute of Aeronautics and Astronautics, Inc, Reston, VA, 2009.

- [21] Pamadi, B. N., *Performance, Stability, Dynamics and Control of Airplanes*, 3rd ed., American Institute of Aeronautics and Astronautics, Inc, Reston, VA, 2015.
- [22] Gur, O., Mason, W. H., and Schetz, J. A., "Full-Configuration Drag Estimation," *Journal of Aircraft*, Vol. 47, No. 4, 2010, pp. 1356–1367. https://doi.org/10.2514/1.47557.
- [23] Nicolai, L. M., and Carichner, G. E., Fundamentals of Aircraft and Airship Design Volume 1 Aircraft Design, American Institute of Aeronautics and Astronautics, Inc, Reston, VA, 2010.